

ChemComm

Accepted Manuscript



This is an *Accepted Manuscript*, which has been through the Royal Society of Chemistry peer review process and has been accepted for publication.

Accepted Manuscripts are published online shortly after acceptance, before technical editing, formatting and proof reading. Using this free service, authors can make their results available to the community, in citable form, before we publish the edited article. We will replace this *Accepted Manuscript* with the edited and formatted *Advance Article* as soon as it is available.

You can find more information about *Accepted Manuscripts* in the [Information for Authors](#).

Please note that technical editing may introduce minor changes to the text and/or graphics, which may alter content. The journal's standard [Terms & Conditions](#) and the [Ethical guidelines](#) still apply. In no event shall the Royal Society of Chemistry be held responsible for any errors or omissions in this *Accepted Manuscript* or any consequences arising from the use of any information it contains.

Direct Measurements of Particle-Surface Interactions in Aqueous Solutions with the Total Internal Reflection Microscopy

Xiangjun, Gong, Zhaohui Wang and To Ngai*

Department of Chemistry, The Chinese University of Hong Kong, Shatin, N.T., Hong Kong.

Abstract : The non-covalent intermolecular forces, such as van der Waals, electrostatic, steric, and hydrophobic/hydrophilic interactions, have played an essential role in determining the association, aggregation, adhesion and sedimentation processes of colloidal particles, surfactant micelles, macromolecules in solutions, or biological systems. These interaction forces, however, are normally weak ($< \text{pN}$) that are challenging and difficult to be directly measured by common force techniques. In this feature article, we discuss recent advances in the development of non-intrusive optical technique of Total Internal Reflection Microscopy (TIRM) for studying the interactions between a single, colloidal particle and a flat surface. We begin with a brief overview of quantitative optical microscopy measurements of particle-surface interactions in aqueous solutions, and then show recent developments associated with TIRM for measuring kT -scale interactions between a single particle and surface in presence of polymer chains, micelles, and colloidal particles with different softness based on our recent work. We also highlight how TIRM can be used to measure the particle-surface interactions after the particle and the flat surface are physically adsorbed or grafted densely with polyelectrolytes, as well as to investigate the non-specific and specific interactions between proteins and protein-carbohydrate in biological systems. Lastly, we conclude with some perspectives on future research efforts in this field.

* To whom correspondence should be addressed.

Email: tongai@cuhk.edu.hk; Tel: (852)-3943 1222, Fax: (852)-2603 5057

1. Introduction

Colloidal suspensions, which are produced by suspending particles/macromolecules with a size range between nanometers to micrometers in solvents, are often encountered in our daily life such as milk, cosmetics, pigments, and inks¹. One of the important properties for the performance and storage life of these colloidal products is their stability, which governs by mutual interaction forces acting between colloidal particles in aqueous environments. The most relevant interaction forces are often rationalized within the classical theory from Derjaguin, Landau, Verwey, and Overbeek (DLVO)¹⁻³, which stipulate that interaction forces can be approximated by the sum of electrostatic double-layer repulsion and van der Waals dispersion interactions. In some situation, other interaction forces, like the steric repulsion due to adsorbed polymer layers, or depletion forces induced by suspended particles and polymers, may also become important^{4, 5}.

On the other hand, in many industrial formulations and biological systems such as red blood cells and living cells, coexisting colloidal and macromolecular components are ubiquitous. It is known that in such mixtures, the presence of macromolecular components such as nanoparticles or polymers can significantly affect the dynamics and phase behavior of the colloidal systems⁶. Nonadsorbing nanoparticles or polymers can be depleted from the regions between colloidal particles and surfaces, producing a local osmotic pressure difference that in turn results in an effective attraction between the colloidal particles and surfaces. This so-called depletion interaction was first described by Asakura and Oosawa (AO) and was studied extensively in complex fluid mixtures as well as were speculated to be widely popular in biological interactions^{7, 8}. Experimental measurements of depletion force has been reported in the past decades by employing, for instance, atomic force microscopy (AFM)⁹, optical tweezers¹⁰, surface force apparatus (SFA)^{11, 12}, and total internal reflection microscopy (TIRM)¹³⁻¹⁶. Among them, TIRM seems to be the most proper technique for measuring such kT -scale depletion potentials due to its passive nature and high sensitivity.

When macromolecular components like polymers are physically adsorbed or grafted densely on the colloids and surfaces, their chain conformations can be assumed to be in three different structures, including mushroom, pancakelike, or stretched brushes, depending on the grafting density and absorption affinity of the polymer segments. Theoretically, polymer adsorption and the interaction between polymer-coated surfaces are often studied using mean field (MF) theories or via computer simulations. Polymer adsorption often results in either stabilization or flocculation, depending on a number of parameters such as solvent quality, the amount of polymer adsorbed to the surface, and whether they are physically or chemically attached to the surface.^{17, 18} Adsorption stabilization, also termed steric stabilization, arises in a good solvent and can be attributed to the osmotic interactions between the polymer segments on opposite surfaces¹⁹. Earlier studies have measured such steric effects between various extending polymer layers by employing SFA²⁰, AFM²¹ or TIRM^{22, 23}. Conversely, adsorption flocculation occurs either due to bridging of polymer chains adsorbed on both surfaces when the polymers prefer the surfaces and there is not enough polymer to fully cover the surfaces, or due to bad solvent conditions for the adsorbed polymer layers⁶. However, the adsorption of macromolecular components at the solid–liquid interface is somehow complicated because this involves several distinctly different processes, including: diffusion in solution, molecular attachment onto the surface, and conformational relaxation of the polymer being adsorbed. Therefore, the experimental study of the polymer-mediated interactions between surfaces can be unambiguously distinguished.

Although theoretical predictions are capable of rationalizing interaction forces in a wide variety of colloidal mixtures, quantitative measurements of such interaction forces acting between colloidal particles across aqueous solutions remain limited and challenging. This can be related to the fact that these interaction forces are normally too weak ($< \text{pN}$) to be detected by traditional force techniques. First direct force measurements involving colloidal particles with the AFM were independently realized by Ducker²⁴ and Butt²⁵. In the meantime, other techniques permitting force

measurements such as optical tweezers techniques and TIRM have been developed²⁶⁻²⁸. Particularly, TIRM is able to monitor the instantaneous separation distance between a large, free-moving spherical particle (few micrometers) and a flat surface. From the equilibrium distribution of separation distances sampled by the Brownian motion, one can determine the potential energy of interaction between the two surfaces. Compared with the mentioned force-measurement techniques like SFA and AFM, TIRM is non-invasive, and provides a better force resolution.

While TIRM is not being widely used in laboratories worldwide, it is probably fair to state that TIRM is ideally suited to measuring extremely weak and dynamic interactions that are most relevant to the stability of colloidal dispersions and interaction of biomacromolecules. Moreover, recent advancements such as the integration of TIRM and video microscopy (VM) enables the simultaneous measurements of many particles at many different surface locations, which generates significantly more statistical information and allows measurements of colloid-surface and colloid-colloid interactions in the same ensemble^{29, 30}. Furthermore, magnetic tweezers has been incorporated in the TIRM that enables measuring of viscoelastic properties of soft materials near solid surface³¹.

In this feature article, we first provide a brief overview of the principle of TIRM and theoretical description of the particle-surface interactions in the aqueous solutions. We then discuss recent experimental explorations in the use of TIRM to non-intrusively measure particle-surface interactions mediated by the presence of different kinds of macromolecular components, including neutral polymer chains, micelles, and nanoparticles with different softness based on our recent work. We also discuss measuring of particle-surface interactions after the colloids and surfaces are physically adsorbed or grafted densely with polyelectrolytes, as well as investigating the non-specific and specific interactions between proteins and protein-carbohydrate in some biological systems. Finally, we provide a summary and some perspectives on future research efforts in this field.

2. The TIRM Technique

TIRM is a relative new technique used to measure directly the mean potential of the interaction between a microscopic colloidal particle and a glass plate. The details regarding to TIRM and its application in measuring different colloidal, surfaces, and external forces can be found in several reviews^{14, 28}. Briefly, when a laser beam is reflected at an angle $\theta > \theta_C$, (with θ being the critical angle of total internal reflection) at the interface between a glass plate and the colloidal suspension, an evanescent light field is created which leaks into the suspension (Fig. 1a). The intensity of the evanescent field is well known to decay exponentially with a penetration depth β^{-1} , which is a function of θ and the refractive indices of the materials comprising the interface. When a colloidal particle approaches the surface close enough to enter the evanescent field, it will scatter light (Fig. 1b). The scattered intensity $I(h)$ from the colloidal particle is collected by an objective and recorded by a photomultiplier tube (PMT) (Fig. 1c). As $I(h)$ of the colloidal particle has been shown to be proportional to that of the evanescent wave, it can be written as²⁸

$$I(h) = I_0 \exp(-\beta h) \quad (1)$$

where h is the distance from the colloidal particle to the slide surface, I_0 is the “stuck” particle intensity, which can be obtained by salting out the particle on the bottom slide surface in the final stage of the experiments, i.e., $h = 0$, and β^{-1} is the characteristic penetration length. By measuring $I(h)$, which fluctuates due to Brownian motion, of the colloidal particle perpendicular to the surface as a function of time thus provides a sensitive and non-intrusive method to determine the distance h between the colloidal particle and the slide surface. In thermal equilibrium the probability distribution $p(h)$ of finding the particle a certain distance to the slide surface is given by the Boltzmann distribution³²

$$p(h) = A \exp\left[-\frac{\Phi(h)}{k_B T}\right] \quad (2)$$

where A is a constant normalizing the integrated distribution to unity. Therefore, the overall interaction potential $\Phi(h)$ between the particle and the surface can be obtained by inverting the distribution (Fig. 1d).

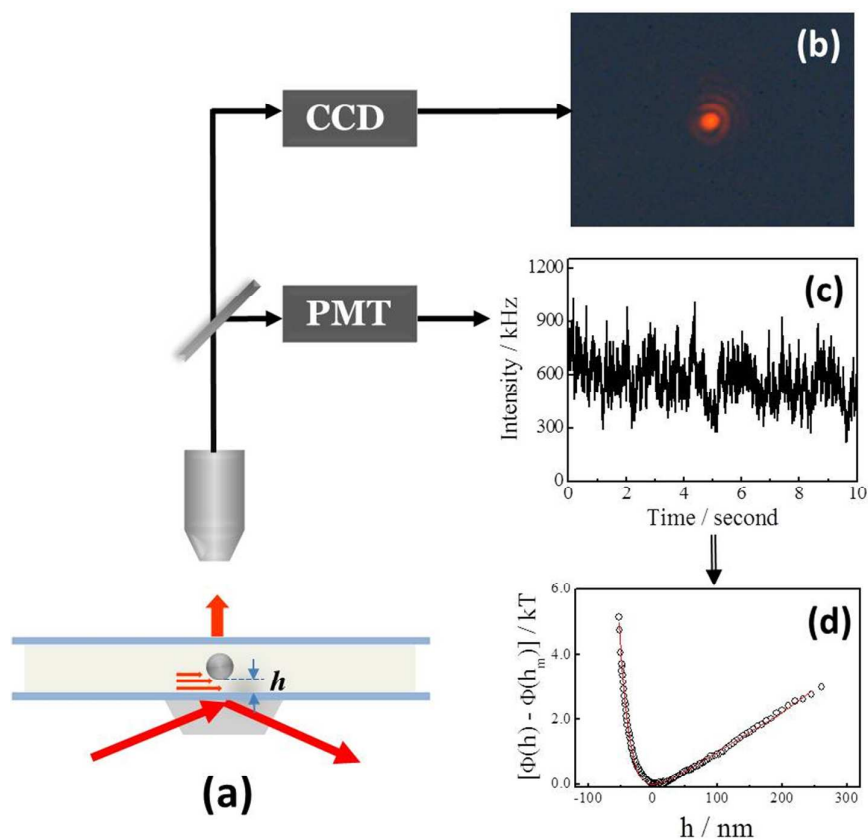


Fig.1 (a) Schematic of a typical TIRM setup: a Brownian colloidal particle moves in the evanescent field generated by total internal reflection at the glass/liquid surface and the scattering intensity from the particle is collected by an objective and recorded by a photomultiplier tube (PMT). (b) Image of a selected polystyrene latex particle (PS) with diameter around $6 \mu\text{m}$ in 0.2 mM sodium chloride (NaCl) taken under evanescent waver illumination. (c) Typically recorded scattering intensity from the Brownian motion of the particles as a function of time. (d) Typical measured interaction potential of a PS particle with a diameter around $6 \mu\text{m}$ and a flat surface in 0.2 mM NaCl aqueous solution.

3. Particle-Surface Interactions Mediated by the Presence of Macromolecules and Nanoparticles in Aqueous Solutions

3.1 Theory

In a typical TIRM measurement, interactions between a Brownian micron-sphere (i.e., PS latex, silica particle) and a glass surface in aqueous solution is profiled. For charged surfaces in aqueous solution with simple electrolytes, i.e., sodium chloride (NaCl), based on the DLVO theory, there should be only two contributions to the measured potential curve: the gravitational energy $\Phi_G(h)$ of the micron-sphere and the double layer repulsion $\Phi_{el}(h)$. As a result, the total potential energy can be expressed as²⁶⁻²⁸

$$\Phi_{tot}(h) = \Phi_G(h) + \Phi_{el}(h) = G_{eff}h + B \exp(-\kappa h) \quad (3)$$

Here κ^{-1} is the Debye length defined by

$$\kappa = \left(\frac{e^2 \sum_i n_i^0 z_i^2}{\epsilon kT} \right)^{1/2} \quad (4)$$

where n_i is the concentration and z_i is the valence of ion of type i . On the other hand, G_{eff} is the effective gravity of the probe particle in the medium and can be expressed as

$$G_{eff} = \frac{4}{3} \pi a^3 (\rho_p - \rho_f) g \quad (5)$$

where a is the radius of the particle, ρ_p is the density of the particle while ρ_f is the density of the fluid, and g is the acceleration due to gravity. B is a function depends on the surface potential between the surface and particle defined as

$$B \equiv 16 \epsilon a \left(\frac{kT}{e} \right) \tanh\left(\frac{e\psi_1}{4kT}\right) \tanh\left(\frac{e\psi_2}{4kT}\right) \quad (6)$$

where e is the electronic charge, ϵ is the relative permittivity, ψ_1 , and ψ_2 are the Stern potentials of the particle and the plate respectively. Eq.(3) is shown to be valid when $a \gg h \gg \kappa^{-1}$, and Fig.1d shows a typical potential profile between the PS particle and the glass slide that is well fitted by Eq. (3) in 0.2 mM NaCl solution. Furthermore, Eq.(3) has a minimum at a separation distance h_m where the derivative of the potential energy equals to 0, and given by

$$\kappa h_m = \ln \frac{\kappa B}{G_{eff}} \quad (7)$$

From Eq. (7),

$$B = \frac{G_{eff}}{\kappa} e^{\kappa h_m} \quad (8)$$

Eliminating B by Eq.(8), Eq. (3) can be converted as

$$\frac{\Phi_{tot}(h) - \Phi(h_m)}{kT} = \frac{G_{eff}}{\kappa kT} \{ \exp[-\kappa(h - h_m)] + \kappa(h - h_m) - 1 \} \quad (9)$$

Here $\Phi(h_m)$ is the potential energy at h_m . Usually, $\Phi(h_m)$ is assumed as zero in TIRM measurements.

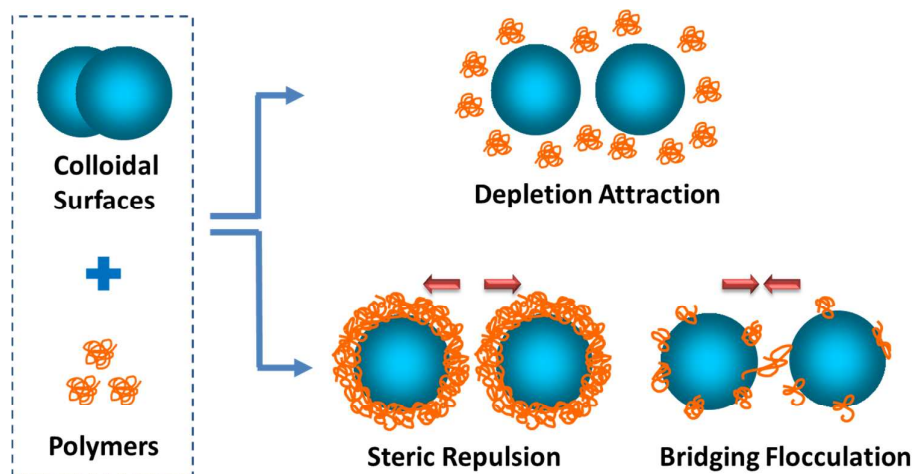


Fig.2 Schematic of polymer-induced interactions between colloidal surfaces. Depends on whether adsorption of the polymers exists on the surfaces, the induced interaction can be either depletion attraction for unabsorbing polymers, or steric repulsion/bridging flocculation for adsorbing cases.

On the other hand, the presence of the macromolecules or nanoparticles in the aqueous solution can significantly alter the interaction profile between the two surfaces. Depending on whether the existing components adsorb on the surfaces as schematically illustrated in Fig. 2, the induced interaction can be either attractive or repulsive. For presence of non-adsorbing polymers, depletion interaction usually takes

place if the size of the polymers is larger than the separation between the two surfaces (h). This is an entropy-driven phenomenon which was first described by Asakura and Oosawa (AO model) in 1954 as mentioned above³³. When individual polymers or nanoparticles cannot enter the space between the two surfaces, they tend to “deplete” between the colloidal surfaces to gain more conformational entropy, which results in an osmotic pressure imbalance (Π) inside and outside the gap and leads to depletion attraction between the two surfaces. The entropic depletion force plays a key role in many industrial processes, biological interactions, and in the formation of special material structures. An outstanding advantage in using depletion forces for control and assembly is that the interaction potentials are easily controlled in the weak-attraction regime, namely, 1-5 $k_B T$. Since the interaction force is so weak, reports of direct observations of depletion appeared only in the recent two decades, owing to the development of highly-sensitive force techniques such as TIRM^{14, 34}, SFA¹², AFM³⁵ and optical tweezers¹⁰.

Depletion interaction $\Phi_{dep}(h)$ with overlapped depletion volume V_{dep} between the spherical PS particle and the flat surface in TIRM measurement is defined as ΠV_{dep} . According to a classic AO model which is valid for non-adsorbing spherical depletants, $\Phi_{dep}(h)$ thus can be represented as^{36, 37},

$$\begin{aligned} \Phi_{dep}(h) &= -\pi\Pi[(a+\Delta)(h-2\Delta)^2 + \frac{1}{3}(h-2\Delta)^3] \quad \text{for } 0 < h < 2\Delta \\ &= 0 \quad \text{for } h > 2\Delta \end{aligned} \quad (10)$$

where Π is the osmotic pressure of the bulk solution, a is the radius of the colloidal particle and 2Δ is the depletion region. It should be noted that Eq.(10) is a approximated formula as the depletants are treated as ideal hard spheres. This equation also ignores the shape, polydispersity of the depletants, as well as interactions between the depletants. Therefore, a number of theoretical methods have been developed to describe the depletion interactions induced by different types of depletants^{15, 30, 38, 39}.

With the presence of adsorbing polymers, either bridging attraction or steric repulsion appears depending on the formation dynamics of the adsorbed layer of the macromolecules. If the surfaces are saturated by adsorbed polymer chains, and the polymer between the surfaces can equilibrate with polymer in the bulk solution at all surface separations, the forces between two adsorbed polymer layers are attractive by the polymer bridging in between due to affinity of polymers to surfaces¹⁷. If the surfaces are under constrained equilibrium, the amount of adsorbed polymer is kept constant, and remains kinetically trapped between the two approaching surfaces, steric repulsion appears due to the overlapping of the polymer layers. Especially, if the polymers detach very slow, or even grafted onto the surface, they act as stabilizers of the surfaces in the good solvent regime, and the interaction between can be described by the classic Alexander-de Gennes model for polymeric brushes.

In this model, it was claimed that each grafted polymer could be considered as a chain of blobs with each of size s , and if it stretched away from the surface in good solvent, the equilibrium layer thickness L can be given by⁴⁰

$$L = s(R_F / s)^{5/3} \quad (11)$$

Thus, the interaction pressure between two identical brushes P_{symm} was presented as a function with the chain s per area, the brush thickness L , and the distance D as¹⁷

$$P_{symm}(D) = \frac{k_B T}{s^3} \left[\left(\frac{2L}{D} \right)^{9/4} - \left(\frac{D}{2L} \right)^{3/4} \right] \quad D < 2L \quad (12)$$

Considering the interaction between a sphere and plate, using Derjaguin approximation $F(D) = 2\pi R \bullet W(D)$ ⁴¹, Block *et al* intergated the pressure in Eq.(12) and got⁴²

$$\frac{F_{symm}(D)}{2\pi R} = \frac{8k_B T L}{35s^3} \bullet \left[7 \left(\frac{2L}{D} \right)^{5/4} + 5 \left(\frac{D}{2L} \right)^{7/4} - 12 \right] \quad (13)$$

When at intermediate surface separations ($0.2 < D/L < 0.9$), Eq.(13) can be well approximated by an exponential decay function with a decay length given by $\gamma^{-1} = -L/\pi$ (symmetric) which depends only on the brush thickness L ⁶.

$$E_{symm}(D) = E_0 \exp(D / \gamma) \quad \gamma^{-1} = -\frac{L}{\pi} \quad (14)$$

3.2 Neutral Polymer Systems

Since electrostatic interaction plays vital role among interactions in soft matter systems, we divided our discussion into two parts: neutral and charged systems. Concerning the neutral polymer systems, one of the most typical polymers is polyethylene oxide (PEO). It is a nonionic polymer that is highly soluble in both aqueous and organic solvents. Therefore, combined with its high biocompatibility, it has been considered as a popular model polymer to mediate the interaction between the solid surfaces and applied in various fields, especially in biological applications such as drug encapsulation⁴³, and antifouling applications⁴⁴. Direct force measurements have been performed to evaluate the interactions mediated by the presence of PEO chains, but the information available in the literature is rather conflicting. For instance, Ohshima *et al.*¹⁰ utilized laser radiation pressure to directly measure the interactions between a colloidal particle and a glass surface in a PEO solution. An attractive force, which was attributed to the depletion force, was found. The measured force could be well fitted by the simple AO theory, but the magnitude was larger than the predicted one. Bechinger *et al.*⁴⁵ performed measurements on the interactions between a charged polystyrene (PS) particle and a glass surface in dilute PEO solutions with TIRM under similar conditions that were conducted by Ohshima *et al.*. They also concluded the occurrence of depletion force induced by free PEO chains in bulk solution. Moreover, they found the resulting interaction potentials were strongly dependent on PEO polymer concentration. However, depletion interaction was not observed by Kleschanok *et al.* in the same system using TIRM²³. Conversely, a steric repulsion due to the formation of a brushlike PEO layer on the PS particle and the glass surface was proposed. Therefore, a systematic exploration of the particle-surface interaction induced by the presence of PEO polymers in water environment provides an essential insight into PEO-mediated industrial formulations and biological systems.

Wei *et al.* systematically measured the interactions between a polystyrene (PS) microsphere and a flat hydrophilic surface in the presence of PEO polymer solution

over a broad range of concentration using TIRM⁴⁶. PEO was shown to be slightly adsorbed onto both PS and glass surfaces. The results reveal that PEO significantly mediates the interactions between the two surfaces. As shown in Fig.3, at dilute polymer concentration ($C/C^* \leq 0.51$), the interactions between the particle and surface are still dominated by repulsive forces originating from double layer repulsion, in line with the classical DLVO theory (Fig. 3(a)); At intermediate polymer concentration ($0.51 < C/C^* \leq 0.85$), beside the double layer repulsion, a long-ranged and weak attraction was detected, which is enhanced as concentration increases (Fig. 3(b)). The measured attractive force is mainly attributed to depletion interaction but the resultant depletion interaction is not compatible with the simple AO model as Eq.(10) described. The reason is attributed to the fact that the size of the polymer chain can no longer be used to represent the characteristic length of this system as concentration increases, and the polydispersity as well as the soft nature of the polymer chains that are not included in the simple AO models; At high polymer concentration where PEO chains overlap, the attraction disappears, and levitation of the microsphere probe is detected. At this overlapping region, the correlation length of PEO chains is much smaller than the size of single PEO molecule, leading to weakening and disappearing of the depletion attraction. Furthermore, at higher polymer concentration ($1.70 \leq C/C^* \leq 2.56$) as shown in Fig 3(c), the attraction becomes weak and finally vanishes, while a short-ranged repulsion rises up. This is because at high concentration regime, PEO chains are highly overlapped so that the static correlation length of this system becomes much smaller. As a result, PEO chains are able to enter into the gap region between the two surfaces and lower the osmotic pressure, resulting in the greatly decrease of the depletion attraction. Finally, Fig. 3(d) shows that at very high concentration ($C/C^* \sim 3.40$), oscillatory structural force is found and the observed spatial correlation length of the polymers decreases as the polymer concentration increases. Therefore, this systematic study clearly presented the influence of PEO concentration onto the interactions of aqueous colloidal systems, and thus showed promising implications for further design and controlling the interactions between surfaces coated with non-ionic polymers.

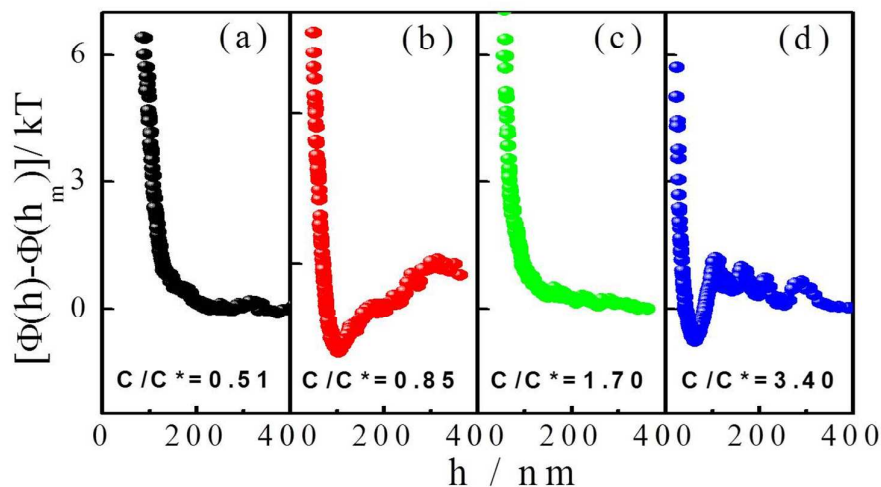


Fig. 3 Potential profiles between the PS latex and the glass slide in PEO aqueous solution with increasing PEO concentrations from (a) to (d) where the gravity part have been all removed. As shown, PEO significantly varies the interaction forces between the two surfaces. At low polymer concentration shown in (a), the interaction between two surfaces in the presence of PEO is mainly dominated by repulsive forces, originating from diffuse layer overlap. As polymer concentration increases, a long range depletion attraction sets in as shown in (b). However, when the concentration continues to increase, the attraction greatly decreases as (c). At very high concentration, oscillatory structural force is detected as shown in (d). (Adopted and reproduced with the permission from ref. 46. Copyright (2013) American Chemical Society.)

3.3 Soft Nanoparticles: Core-Shell Particles, Microgels, Micelles and Nanobubbles

Compared with neutral polymers, charged soft matters are more commonly seen in practical applications. However, charging enhances the electrostatic repulsion, and leads to long range correlations, which thus competes with the influence induced by structural softness and makes the case much more complicated. Nevertheless, charged materials with soft nature, i.e., core-shell particles with a solid core surrounded by a

soft shell, microgels, micelles and even nanobubbles have been shown to play important roles in mediating interactions and phase behavior of aqueous colloidal systems which are apparently distinguished with hard particles. For better understanding, in this section, the measurement of the interactions induced by these particles are introduced in a sequence with increasing softness.

Xing *et al.* measured and compared the interaction potential energy profiles between a micron PS particle and a plate surface induced by both hard-spheres (highly charged PS nanoparticles) and core-shell nanoparticles (weakly charged, PS nanoparticles as core and poly(*N*-isopropylacrylamide) (PNIPAM) hydrogel as shell) with similar size in the dependence of volume fraction of the added nanoparticles in diluted region⁴⁷. For the hard-sphere nanoparticles, the interaction showed a monotonous dependence with the nanoparticle concentration, i.e., the separation distance between the two macron surfaces is substantially increased above that with no nanoparticles, and an increasing amplitude of a net weak attraction $\sim k_B T$ was found as concentration of nanoparticles increases. For the core-shell nanoparticles, Fig. 4 shows the interaction potentials measured at solutions containing such PS-co-PNIPAM core shell nanoparticles with different volume fractions. The effect of adding core-shell nanoparticles to the solution is summarized as follows: (i) At a low volume fraction $\phi_{\text{nanoparticle}} (< 2 \times 10^{-4})$, the addition of core-shell nanoparticles has a much smaller impact on the interaction potential profiles. (ii) At an intermediate core-shell nanoparticle volume fraction ($2 \times 10^{-4} < \phi_{\text{nanoparticle}} < 5 \times 10^{-4}$), separation distance, h , decreases with an increasing nanoparticle volume fraction and the measured interaction potentials are shifted closer to the plate surface, indicating that a long-range attractive force is generated. They inferred the attraction due to the deposition of weakly charged nanoparticles onto the highly charged surfaces, which reduces the electrostatic interaction between the nanoparticle-decorated microparticle and plate surfaces and causing weak bridging. (iii) At a high core-shell nanoparticle volume fraction ($\phi_{\text{nanoparticle}} \geq 8 \times 10^{-4}$), h is surprisingly increased, suggesting an enhanced repulsive force in the system. The authors proposed one possible reason for

this repulsion that when more core-shell nanoparticles were added, the surface of both the microparticle and plate may be better covered by the deposited nanoparticles. This soft layer nanoparticle can sustainably generate a steric repulsive force to overwhelm the attraction and plays the role as stabilizer. These results showed that due to the existence of adsorption between the colloid and the soft core-shell nanoparticles, the interactions between colloids and surfaces were tuned by the adsorbed nanoparticles, which lead to either attraction or repulsion due to the adsorbed amounts and configurations.

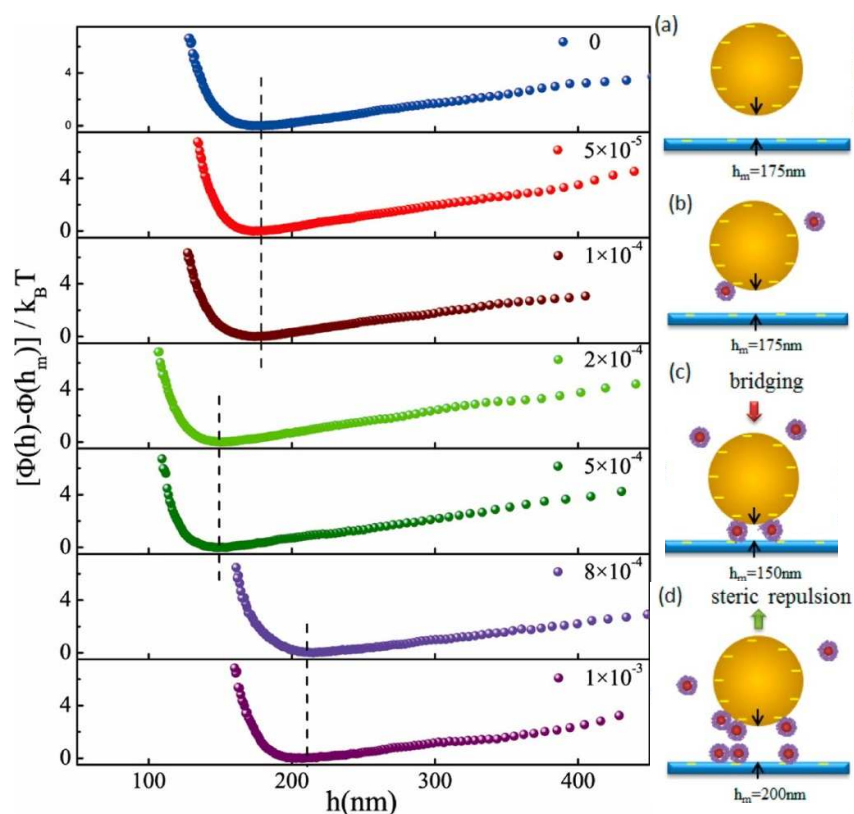


Fig. 4 Measured interaction potential profiles and corresponding schematic diagram of the interactions between the microparticle and glass substrate at varying PS-co-PNIPAM core-shell nanoparticles volume fractions with solution pH 10.25. (a) initial conditions, (b) core-shell particles slightly adsorbing to the microparticle or plate at a low volume fraction of the core-shell particles, (c) attraction by bridging

between the microparticle and plate at a medium volume fraction of the core-shell particles, and (d) steric repulsion induced by abundant adsorption between the microparticle and plate at a high volume fraction of the core-shell particles. (Adopted and reproduced with the permission from ref. 47. Copyright (2012) American Chemical Society.)

Compared to PS-*co*-PNIPAM core-shell nanoparticles, another kind of nanoparticles which have a higher softness and stimuli response, poly(*N*-isopropylacrylamide-*co*-methacrylic acid) (PNIPAM-*co*-MAA) microgel particles, were also used to explore the induced interactions to colloidal systems employed with the TIRM techniques. Xing *et al.* presented the first study of the depletion potentials between PS colloidal sphere and a flat wall in the presence of PNIPAM-*co*-MAA microgel particles at diluted aqueous solution.⁴⁸ In this study, microgel particles were designed as the depleting agents due to the fact that such microgels exhibit dramatic changes in particle diameter from 254 to 216 nm as pH changes from 9.5 to 4.6. As shown in Fig.5, the interaction potentials between the PS sphere and the flat surface in the presence of swollen microgel particles could be significantly varied from attractive (pH = 9.4) to purely repulsive (pH = 4.5). It clearly shows that the addition of swollen microgels (curves at pH = 9.4) induces a long-range attractive force occurring at separation distances ranging from 150 to 250 nm. This attractive force is seen to increase with increasing swollen microgel concentration, while the separation distance decreases. Moreover, at higher swollen microgel volume fractions, the attractive well becomes narrow and steep as well as acting over smaller separation distances. Since the microgels, the selected PS sphere and the hydrophilic glass surface are all negatively charged under the experiment conditions, the microgels would not preferentially absorb to either the PS sphere or glass surface. Consequently, depletion interaction was responsible for the attraction. A fit by Eq.(10) of the net microgel-induced depletion potential at pH = 9.4 obtained by subtracting the potential curve at pH 4.5, they found that the depletion region $2\Delta \sim$

250 nm, close to the hydrodynamic diameter of the swollen microgels, and $\Pi \sim 0.4$ Pa suggesting that the experimental results are in good agreement with the theoretical values predicated by classical description of depletion. This agreement further indicated that, in diluted region, charged soft particles behave as hard spheres. As a result, this study showed a quantitative measurement of $k_B T$ -scale depletion attraction by using soft nanoparticles.

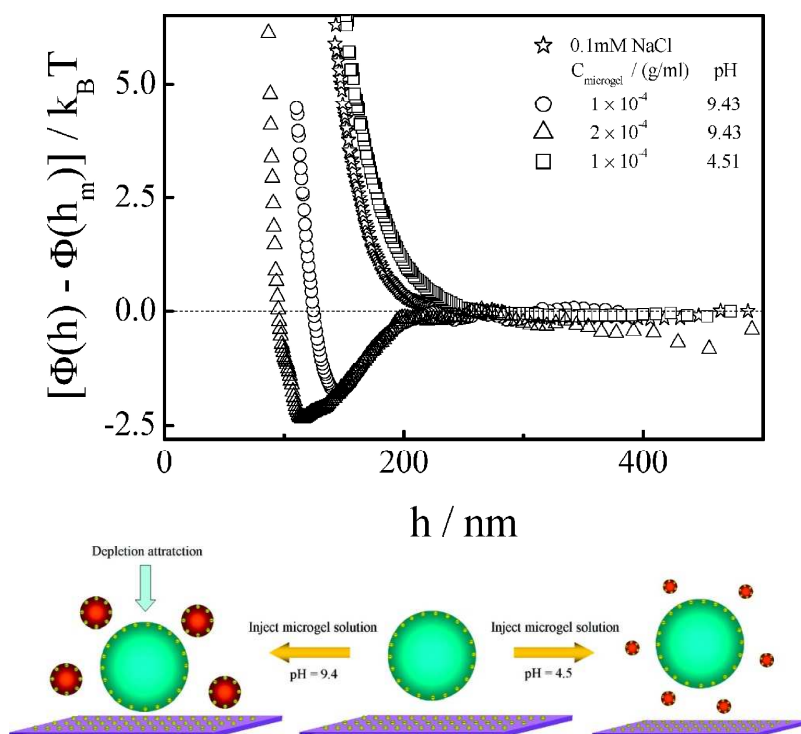


Fig. 5 Above: Measured interaction potentials between the polystyrene sphere and flat surface under different environmental conditions, namely, in 0.1 mM NaCl aqueous solution, in different concentrations of microgel dispersion at pH = 9.4, and in microgel dispersion at pH = 4.5. Note that the gravity of all the interaction potentials has been subtracted. Below: Schematic shows the pH-triggered depletion attraction acting on polystyrene sphere immersed in the microgel dispersion close to a flat surface. (Adopted and reproduced with the permission from ref. 48. Copyright (2009) American Chemical Society.)

Besides the studies on induced interaction in colloidal systems by particles at size scale of ~ 100 nm, interesting explorations on interactions have been performed

on commonly used small molecules, such as α -cyclodextrin (α -CD). α -CD has been proven previously to produce stable nanobubbles in aqueous solution by dynamic light scattering techniques, however, the formed nanobubbles can be removed by repeated filtration (RF).^{49, 50} Jin *et al.* performed the first study to investigate the effects of the presence or absence of such bulk-free nanobubbles on the induced interaction between a free-moving colloidal particle and a flat surface in aqueous solutions of α -CD⁵¹. As can be seen in Fig.6, the total seven measurements of the interaction potentials between the particle and flat surface under different conditions were given. It showed that the three potential curves measured after nanobubbles were produced and removed by RF, all collapsed to a single theoretical curve which can be well described by Eq.(3). The fitting results $G \sim 72$ fN and $k^{-1} \sim 30$ nm, both agreed well with the theoretical values ($G = 70$ fN, $k^{-1} = 30$ nm) as calculated using the known size and density of the PS particles and the electrolyte concentration, revealing that the presence of the free α -CD molecules has little effect on the interaction between the particle and surface. Subsequently, the profiles measured when nanobubbles were not removed was subtracted by the removed profile to obtain the net attraction $\Phi_{\text{Dep}}(h)$ and fitted by Eq.(10). The fitting gives $2\Delta \sim 190$ nm and $\Pi \sim 0.2\text{--}0.3$ Pa. Such a fitted depletion region equals to the sum of diameter of the nanobubbles ($2R_b = 160$ nm) and thickness of the nanobubbles' double layer ($\kappa^{-1} = 30$ nm), indicating that the results are in good agreement with the theoretical values predicated. On the other hand, the obtained Π was unusually high due to the fact that the nanobubbles are highly negatively charged which can dramatically enhance the depletion.^{34, 36, 37, 52} This study quantitatively showed for the first time that the existence of nanosized bubbles (~ 200 nm) in the aqueous solution, like the nonadsorbing polymers and micelles, can induce a depletion attraction $\sim k_B T$ between the particle and the flat surface.

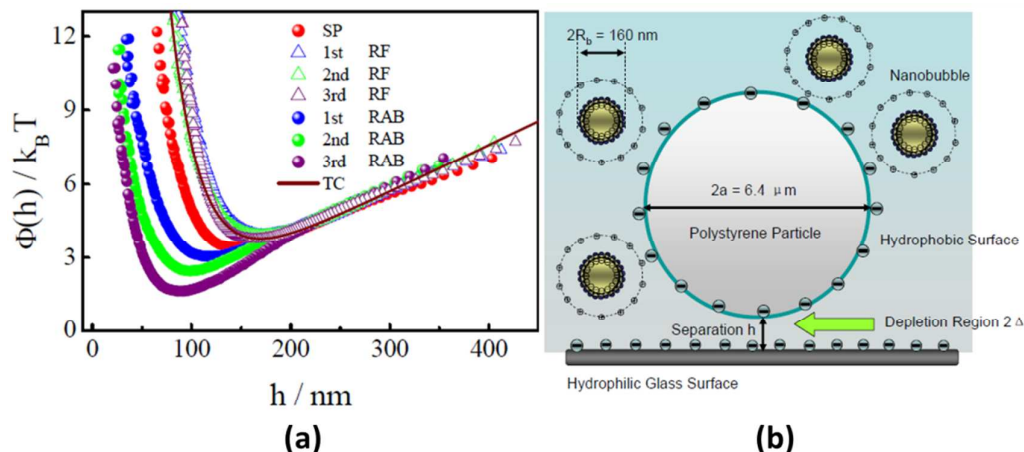


Fig. 6 Measured interaction potentials ($\Phi(h)/k_B T$) between a PS particle and a glass surface both in the presence and absence of nanobubbles. Note that the aqueous solution was firstly filled with spontaneously dissolved α -CD molecules (SP); then it was repeatedly filtrated to remove the nanobubbles (RF); After that, the nanobubbles were reintroduced into the solution by direct air injection (RAB). 1st, 2nd and 3rd represent the corresponding ordinal number. TC is a theoretical curve from Eq. (3) with $k^{-1} = 30 \text{ nm}$ and $G = 70 \text{ fN}$. (Adopted and reproduced with the permission from ref. 51. Copyright (2008) Royal Society of Chemistry.)

Edwards *et al.* gave a comprehensive study on soft particles induced depletion interactions by combining techniques of TIRM, video microscopy (VM) and Monte-Carlo (MC) simulation³⁰. They measured depletion potentials between silica surfaces by TIRM and investigated the related quasi-2D phase behavior by imaging processing and simulation for four different types of materials with varied softness, i.e., charged sodium dodecyl sulfate (SDS) micelles, charged silica nanoparticles, neutral PEO chains, and nonionic PNIPAM microgels. Fig.7a shows that, in all the four cases, the depletion attraction leads to a single energy well with a monotonically increasing depth and decreasing minimum location as the depletant concentration/volume fraction increases. The net attraction curves were accurately fitted by theoretical potentials considering the electrostatic, steric, van der Waals, and

optimized depletion potentials for spheres and polymer chains.^{13, 30} Especially, the net depletion potentials were modified to include following parameters (1) an effective depletant radius, Δ_{EV} , to account for soft depletants for the volume term; (2) a compressibility factor, Z , to account for the osmotic pressure term; and (3) a partition coefficient, $\langle K \rangle$, to account for partial depletion in the volume term. As a result, Δ_{EV} , Z and $\langle K \rangle$ were obtained for each case: for charged SDS micelles and silica nanoparticles, both Δ_{EV} equal to the core size L_{core} plus $4.7\kappa^{-1}$ (κ^{-1} is Debye length) to account for electrostatic interactions; for neutral PEO depletants, Δ_{EV} equals to an factor multiplied by the correlation length of PEO chains; for nonionic PNIPAM microgel depletants, Δ_{EV} equals to its hydrodynamic radius.

On the other hand, Fig. 7b gave (1) VM measured 2D fluid configurations, (2) VM measured 2D crystalline configurations, and (3) radial distribution functions, $g(r)$, from both VM measurements and MC simulations for the conditions corresponding to the images, where MC simulations adopted all the parameters as TIRM results yielded but keeping $\langle K \rangle$ adjustable to fit the VM results well. From the well fitted results as shown in both Fig. 7a and b, the authors argued that the modified depletion equations was able to describe the interactions induced by those common depletants, either charged or neutral, hard or soft.

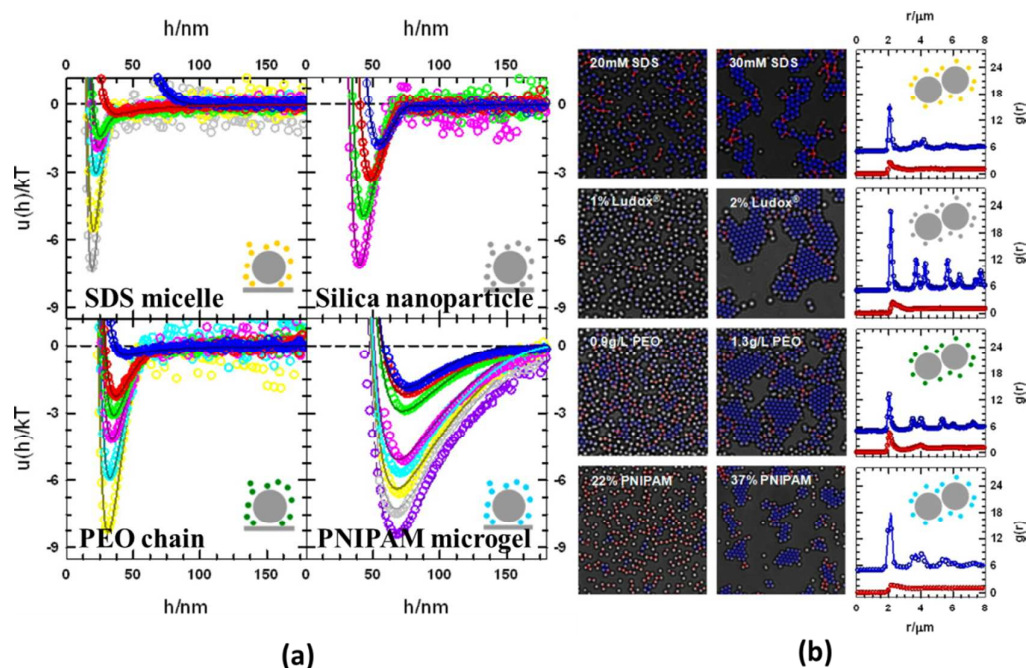


Fig. 7 (a) Depletion potentials between silica particle and surface measured by TIRM of (1) SDS micellar depletants for 1 mM (blue), 6 mM (red), 8.5 mM (green), 10 mM (pink), 12 mM (cyan), 14 mM (yellow), and 16 mM (gray) SDS concentrations (2) SiO₂ nanoparticle depletants with 0.2% (blue), 0.4% (red), 0.6% (green), 0.8% (pink) volume fractions. (3) PEO chains depletants for 5 mM NaCl (blue) and 0.214 g/L (red), 0.321 g/L (green), 0.428 g/L (pink), 0.642 g/L (cyan), and 0.856 g/L (yellow) PEO concentrations. (4) PNIPAM microdrogel depletants for 22 % (20 °C, red), 24 % (22 °C, blue), 26 % (24 °C, green), 28 % (26 °C, pink), 31 % (27 °C, cyan), 34 % (28 °C, yellow), 36 % (28.5 °C, gray), and 37 % (29 °C, purple) PNIPAM particle volume fractions; Noted that the gravity parts have been all removed from the potential curves. (b) (left-to-right) VM measured 2D colloidal configurations as a function of depletant volume fraction for (column 1) dynamic equilibrium quasi-2D fluids; (column 2) crystallites coexisting in dynamic equilibrium with fluid particles; and (column 3) radial distribution functions, $g(r)$, from VM (points) and MC simulations (lines). The images in columns 1 and 2 are processed to show whether bonds between adjacent particles are crystalline (blue) or amorphous (red). Depletant volume fractions in $g(r)$ correspond to those in column 1 (red, bottom) and those in column 2 (blue, top). (Adopted and reproduced with the permission from ref. 30.

Copyright (2012) American Chemical Society.)

3.4 Polyelectrolytes

Polyelectrolytes are macromolecules with ionizable groups along their chains. Addition of polyelectrolytes would predominantly vary the stability and rheology of colloidal suspensions due to the induction of electrostatic interaction and entropic rearrangements of ions and counterions.⁵³ This thus leads to a great difference of involved dynamics and phase behaviors from neutral polymers. As a consequence, polyelectrolytes have been widely applied in industrial applications such as waste-water treatment, papermaking, as well as formulation of foods, paints, or cosmetics.⁵⁴⁻⁵⁷ The measurements of interactions related to polyelectrolytes in colloidal systems give important guidance on further applications of polyelectrolytes.

Concerning the effect of addition of free polyelectrolytes, Gong *et al.* used TIRM to measure the interaction forces between a Brownian colloidal sphere and a flat glass plate in the presence of unadsorbed free cationic poly(ethylenimine) (PEI) chains (molar weight = 25 k g/mol), when both surfaces were saturated with physisorbed PEI chains.⁵⁸ Note that PEI has been widely used to tune the stability, rheology, or adhesion properties of colloidal suspensions due to their strong tendency to adsorb to solid surfaces. It has also gained importance as gene carriers in biomedical applications, in which the anionic DNA chains are complexed and condensed to form PEI/DNA polyplexes. Some reported literatures have recently shown that the overdosed PEI chains, which are free in the solution mixture, also play a vital role in promoting the gene transfection, but the reason is unclear.⁵⁹ Gong *et al.* thus investigated the effect of overdosed free branched cationic PEI polyelectrolytes on the interaction potentials between a colloidal and a glass surface. Fig. 8 illustrates both the salt and free PEI concentration dependence of the induced interaction at low ionic strength solutions. The results showed a reproducible long-ranged attraction (appeared at $h > 60$ nm, ~ 1.5 to $2.0 k_B T$) induced by the addition of free PEI chains at PEI concentrations as low as 10 ppm. Moreover, this attractive force increases with

increasing polyelectrolyte concentration and increasing background electrolyte ionic strength. In addition, decreasing pH value also leads to increase of the attractive force. They argued that the addition of polyelectrolytes, salt, or lowering pH enhanced a net long-ranged attraction, likely related to the reduced electrostatic repulsion between the two PEI bearing surfaces. The contribution from steric and direct bridging forces were shown to be unlikely occurred so that this attractive force might originate from depletion, i.e., the free polyelectrolytes might show a depleted layer much larger than their size due to charging^{38, 60}; On the other hand, varying the environmental conditions leads to the charge redistribution of the inhomogeneous adsorbed polyelectrolyte layers and the related ion-ion correlation in the limited geometry. This study systematically showed that dosing of free cationic PEI leads to a complex interplay of electrostatic interactions between adsorbed polyelectrolyte films and causing net attractive forces.

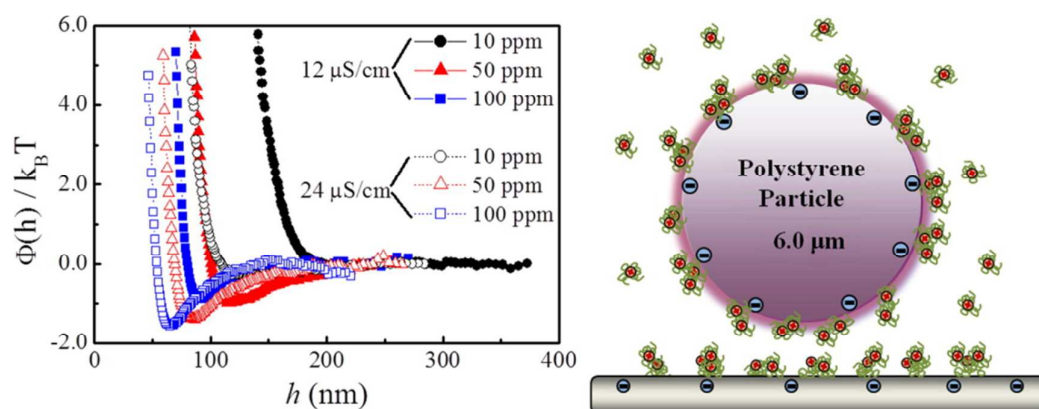


Fig. 8 Net potential energy profiles (Left) and schematic (Right) between the PEI coated sphere and PEI-coated glass surfaces in the presence of different concentration of PEI at 12 and 24 $\mu\text{S/cm}$ ionic strength sodium chloride (NaCl) aqueous solutions. The gravity part of the potential profiles measured in PEI solutions was removed. (Adopted and reproduced with the permission from ref. 58. Copyright (2013) American Chemical Society.)

Wei *et al.* studied the interaction between the surface-grown cationic

poly(2-(methacryloyloxy)ethyl trimethylammonium chloride) (PMETAC) brushes (thickness ~ 25 nm) and a 5 μm diameter positively charged polystyrene (PS) particle in different electrolyte environments (NaCl and NaClO_4) using TIRM.⁶¹ As can be seen in Fig. 9, at the same concentration, NaClO_4 causes a much more abrupt decrease in h between the particle and surface than that with NaCl solution. The author proposed that this observed measurement could be associated with the strong ion-pairing interaction between the ClO_4^- anions and the quaternary ammonium group in the PMETAC brushes, which experienced not only pure charge screening, but also a sharp hydrophilic-to-hydrophobic change of the brush layer.⁶² Therefore, this work showed that TIRM is able to provide a sensitive method to detect such an ion induced collapse transition of surface confined polyelectrolyte brushes, even at very low specific anion concentrations.

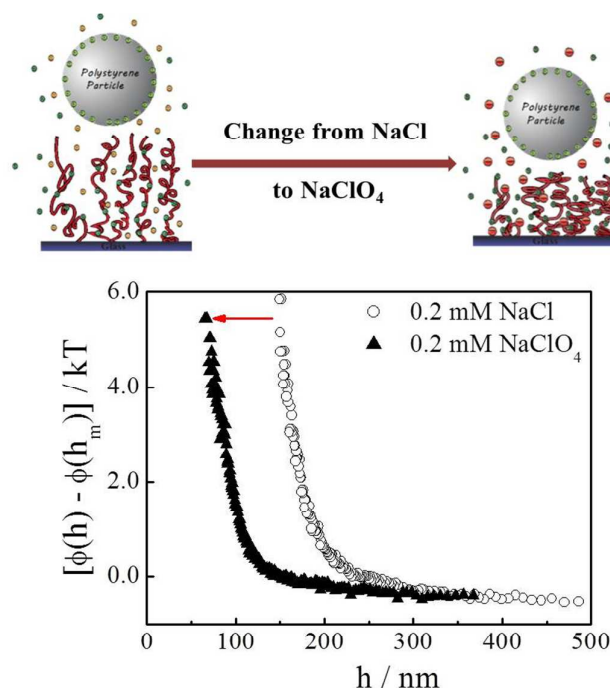


Fig. 9 Schematic (Above) and potential energy (Below) for investigating the ion-pairing induced collapse transition of surface-confined polyelectrolyte brushes at low specific anion concentrations. The gravity part of the potential profiles was removed. (Adopted and reproduced with the permission from ref. 61. Copyright (2012)

Royal Society of Chemistry.

In another work on interactions related with cationic polyelectrolyte brushes, Wei *et al.* presented a study by using TIRM to measure the interaction between poly(2-(dimethylaminoethyl methacrylate)) (PDMAEMA) brushes with two different lengths grafted on a glass slide and a positively charged polystyrene (PS) particle with pre-adsorbed layers of PEI ($M_w = 2000$ g/mol), in aqueous solutions.⁶³ PDMAEMA is a pH-responsive polymer and, at pH 7, the polymer is partially charged (hydrophilic) and partially uncharged (hydrophobic). At lower pH the polymer becomes more positively charged, and at pH values greater than 7 it is mostly uncharged.⁶⁴ PDMAEMA has a wide range of potential uses such as a nonviral gene delivery vector and an ion exchange media for protein separation.^{65,66} In this work, both pH and salt effects were explored for the PDMAEMA brushes with two lengths respectively. For short polymer brushes (~ 30 nm), at pH 4.2 and 3.5 the interaction between the partially protonated and swollen PDMAEMA brush and the positively charged PS particle was dominated by repulsive forces at low salt concentrations, originating from diffuse layer overlap described by Eq.(3). However, when the pH is decreased to 3.0, a long-range attraction sets in. The author speculated the patch-like configuration of the heterogeneous adsorbed PEI on PS should be responsive for the pH induced long-ranged attraction due to the attraction between the brushes and oppositely charged uncovered PS surface and hydrophobic interaction between the uncharged brushes and hydrophobic segments on PS surface (Fig.10).

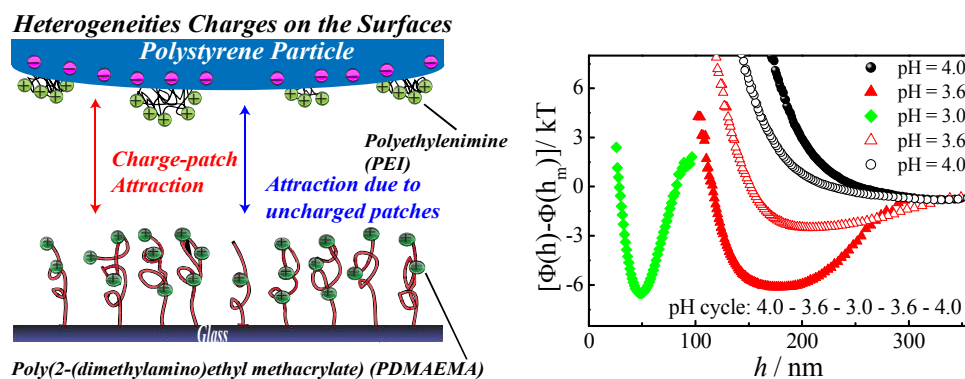


Fig. 10 Left: Schematic illustration of the interactions between the PDMAEMA grafted glass surface and the PEI-bearing PS probe particle. Right: Interaction potentials between the PEI-coated particle and the longer PDMAEMA grafted glass in various pH values aqueous solutions. The five measurements that were performed in a pH cycle: 4.0 – 3.6 – 3.0 – 3.6 – 4.0 by using the same PS particle and the PDMAEMA grafted glass slide (~ 75 nm). Noted that the gravity part of the potential profiles was all removed. (Adopted and reproduced with the permission from ref. 63. Copyright (2013) Royal Society of Chemistry.)

For longer polymer brushes (~ 75 nm), the influences of the pH and salinity were similar but more complex. Fig. 10 summarizes the measurements that were performed in a pH cycle: the interaction between the longer PDMAEMA-grafted surface and the PS particles was measured at pH 4 and then decreased to pH 3.6, 3.0, and switched back to pH 4.0. At the starting pH 4.0, the interaction was analogous to the shorter brushes. As pH decreased, there is a competition between the charging and screening when the pH value of the solutions is lowered. At both the initial and final pH 4.0, repulsive interaction between the brush and the probe PS particles prevails, indicating that charging is important and brushes are in the swollen state. However, at pH 3.6, the attraction sets in. Furthermore, at pH = 3.0, the interaction potential was much narrower with enhanced attraction and repulsion in a shorter range, and the separation distance was down to 50 nm where physical contact between the brush and the particle occurred. At this moment, the steric repulsion sets in. This study indicated that the interaction potentials between polyelectrolyte brushes highly depended on the electrostatic environments, namely, the varying charging of brushes, the variations of the conformation of the brushes, the surface patch-charge heterogeneities, the imbalance causing by the localized counterions near the polyelectrolyte brushes, and the hydrophobic interaction between the hydrophobic areas with the uncharged part on the brushes as well.

4. Interactions in Biological Systems

Besides above studies, TIRM has been utilized in exploration of interactions in biological systems, including both specific and non-specific interactions. Actually, most of the non-specific interactions existing in biological systems are the same interactions commonly found in the polymer/macromolecules systems. Therefore, specific interactions can be obtained if non-specific interactions are well modeled for known total interactions given by TIRM.

4.1 Nonspecific Interactions

Everett *et al* have used TIRM and particle tracking techniques to study protein-protein and protein-synthetic macromolecule nonspecific interactions in phosphate buffer solution (PBS).⁶⁷ Interactions and dynamics between bovine serum albumin (BSA) and copolymers with exposed PEO moieties adsorbed colloidal surfaces were systematically measured. Potential energy profiles of BSA coated colloids-BSA coated surface (BSA-BSA), PEO coated colloids-PEO coated surface (PEO-PEO), BSA coated colloids-PEO coated surface (BSA-PEO) and PEO coated colloids-BSA coated surface (PEO-BSA) were detected.

Fig. 11 shows an example of the results of BSA coated colloids-PEO5k coated surface, in which Fig. 11a presents 25 grey diffusing colloidal trajectories as well as the statistics of the corresponding colloidal-surface association (CSA) time. On the other hand, Fig. 11b shows the combination of colloid-surface van der Waals attraction and nonspecific BSA-PEO5k osmotic repulsion, resulting in a $0.7k_B T$ energy well. Using known PEO5k copolymer brush thickness ~ 20 nm and 14 nm for BSA layer^{22,68}, the start of BSA-PEO repulsion was estimated at 34 nm. On the other hand, fitting of the measured van der Waals minimum using rigorous theory⁶⁹ gave a distance ~ 40 nm as the beginning of repulsion. The authors contributed the difference may be caused by the surface roughness which is likely weaken the van der Waals attraction. Furthermore, lateral diffusion information shown in Fig. 11c provides temporal and spatial consistence with the repulsive potential curves in Fig. 11b. Predicted lateral diffusivities near walls based on colloid-surface hydrodynamic interactions with impermeable adsorbed layers, showed excellent agreement with the

resultant short-time x and y MSDs⁷⁰⁻⁷². Combining all the results, this study reveals how BSA layer and PEO copolymer architectures on substrates with different heterogeneities to influence colloid-surface attraction and association lifetimes. Among them, BSA-BSA, BSA-PEO, and PEO-PEO interactions were completely repulsive such that CSA only occurs due to nonspecific attraction, particularly in the presence of surface heterogeneity. Thus this work quantitatively measures the nonspecific interactions between proteins and synthetic macromolecules, and provides a baseline to differentiate specific and nonspecific interactions between protein binding partners on colloids and surfaces.

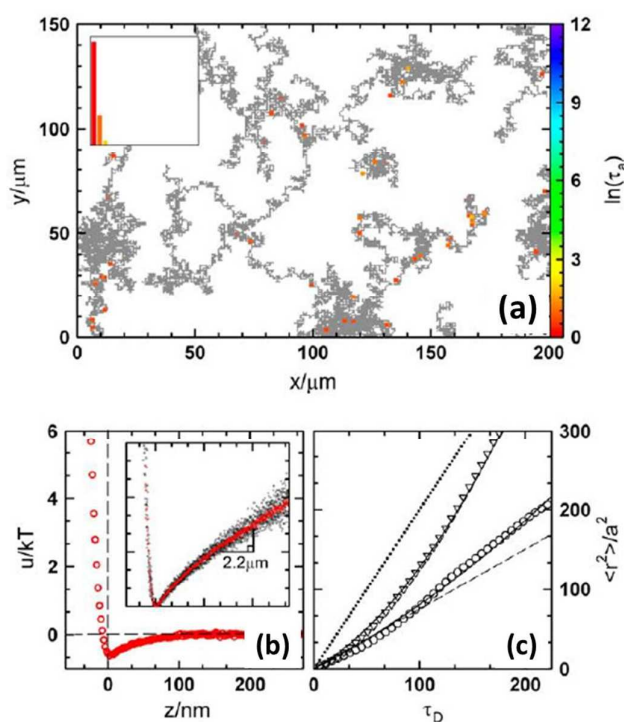


Fig. 11 (a) Trajectories of BSA coated colloids on PEO5k coated glass surface. Gray pixels indicate no colloidal-surface association (CSA), and colored pixels indicate CSA times (right-side scale). (b) Single (black) and ensemble (red) colloid potential profiles without and with (inserted) gravitational potentials. (c) Ensemble average lateral mean-square displacements (MSDs) in x (\circ) and y (\square) directions with curve

fits (solid line), predictions (dashed line), and isolated single colloid diffusion (dotted line.). (Adopted and reproduced with the permission from ref. 67. Copyright (2007) Cell.)

4.2 Specific Interactions

In 2010, Everett *et al* used TIRM and video microscopy to study specific Ca^{2+} -dependent homophilic interactions between lipid bilayer modified SiO_2 colloids (LBCs) decorated with *N*-cadherin and supported lipid bilayers (SLBs) decorated with *N*-cadherin on planar microscope slide surfaces.⁷³ They found nonspecific macromolecular repulsion between cadherin fragments in the absence of Ca^{2+} and irreversible bilayer fusion via cadherin-mediated attraction at $> 100 \mu\text{M}$ Ca^{2+} . Firstly the nonspecific interactions on the condition of either cadherin have been linked or not to the surface were obtained in control experiments. In the absence of Ca^{2+} , the profiles for PEG coated only case and cadherin added case are quite similar shown as Fig.12a, except that the case with the *N*-cadherin shows slightly softer repulsion and less attraction than the PEG-only case. The predicted nonspecific interactions consist of macromolecular osmotic repulsion (steric repulsion) and van der Waals attraction fitted well with Fig.12a and b. After that, Ca^{2+} -dependent *N*-cadherin interactions were measured as Fig. 12c with the concentration of $[\text{Ca}^{2+}]$ at 10 and 100 μM . The results showed that below 10 μM $[\text{Ca}^{2+}]$, the interaction potentials were almost the same with the nonspecific *N*-cadherin profiles in Fig. 12a. But at 10 and 100 μM $[\text{Ca}^{2+}]$, LBCs all attached to the surface and the fusion was irreversibly upon reducing Ca^{2+} or imidazole addition, suggesting adjacent SLBs became fused as part of *N*-cadherin binding at higher $[\text{Ca}^{2+}]$. As a result, this work reported a much lower *N*-cadherin attraction at micromolar Ca^{2+} concentrations than previously reported measurements⁷⁴⁻⁷⁶ which might mainly contribute to the high interaction sensitivity of TIRM techniques.

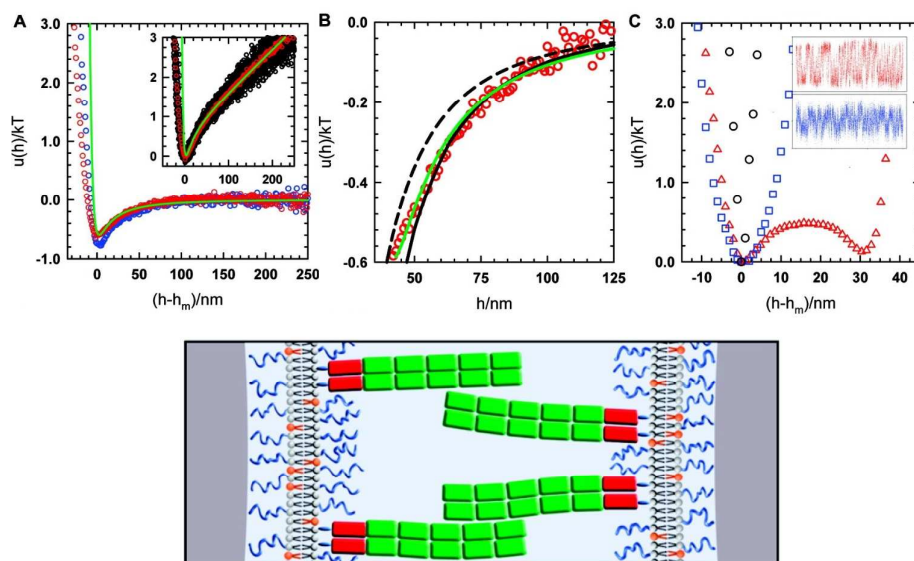


Fig. 12. Above: (a) Ensemble potential profiles between nominal SiO_2 colloids (diameter: 2.1 μm) with SLBs and a microscope slide with SLB before (blue circles) and after (red circles) *N*-cadherin binding. Gravitation was subtracted to clarify the attractive potential, and the inset plot shows the same profiles with the gravitational potentials. The line (green) is the fit to the ensemble average potential (red). (b) Attractive portion of (a) in the top plot with fit (green) and Lifshitz theory with (solid black line) and without (dashed line) consideration of the SLB contribution. (c) Ensemble potential profiles for (○) bare SiO_2 on bare microscope slides in 0.15 M NaCl and for particles and surfaces with *N*-cadherins immobilized on SLB in 0.15 M NaCl with 10 μM $CaCl_2$ (Δ) and 100 μM $CaCl_2$ (\square). Inset shows normalized single particle intensity vs time data for the two cases with same colors as main plot. Below: Schematic cross-sectional view of the SLBs on adjacent micrometer-scale colloidal particles, which is primarily 1-palmitoyl-2-oleoyl-snglycero- 3-phosphocholine (POPC) lipids but also includes sufficient 1,2-diacyl-sn-glycero-3-phosphoethanol amine-*N*-[methoxy(poly(ethylene glycol))-2000] (PEGPE) producing brush structures and 1,2-dioleoylsn-glycero-3-[(*N*-(5-amino-1-carboxypentyl)iminodiacetic acid)-Succinyl] with nickel salt (DGS-NiNTA) lipids conjugated to *N*-cadherin fragments. (Adopted and reproduced with the permission from ref. 73. Copyright (2010) American Chemical Society.)

Furthermore, Eichmann *et al* detected the specific interaction between specific protein conconavilin A (ConA) decorated colloid and polysaccharide (dextran)-functionalized surfaces in the presence of a competing monosaccharide (glucose).⁷⁷ As shown in Fig. 13, with the increase of concentration of glucose, ConA decorated colloidal particles changed from immobilized to dextran functionalized surface to detaching from the surface. For concentration of glucose $[g] = 0$ mM in Fig. 13a, TIRM measurements showed that all particles are localized on the surface due to the ConA–dextran interactions; For $[g] = 5$ mM in Fig. 13b are similar to the potential energy profiles in Fig. 13(a), where almost all the particles were stuck, except that only one particle can move much further above the surface; For $[g] = 10$ mM in Fig. 13c, freely moving, intermittent binding, as well as stuck particles could be all found. Solid lines in Fig. 13c were fitted results by potential model including gravity, van der Waals attraction, steric repulsion and tether potentials by taken a tethered chain as a Hookean spring.^{78, 79} In each case, the theoretical potentials agree well to the measurements; however, as $[g]$ increased to 100 mM in Fig. 13d, most of particles began to freely diffuse with only few tethered ones. The inset of Fig. 13d shows potential profiles for a control experiment with BSA-coated colloids over dextran-coated microscope slides. Both the inset and main plots show the same percentage of freely diffusing ($\sim 85\%$) and tethered ($\sim 15\%$) particle profiles. These results clearly showed that nonspecific repulsion began to dominate in the ConA–dextran interaction in 100 mM glucose as well as in the BSA–dextran interaction and ConA sites appeared to be saturated by glucose so that no bonds could form between ConA and dextran.

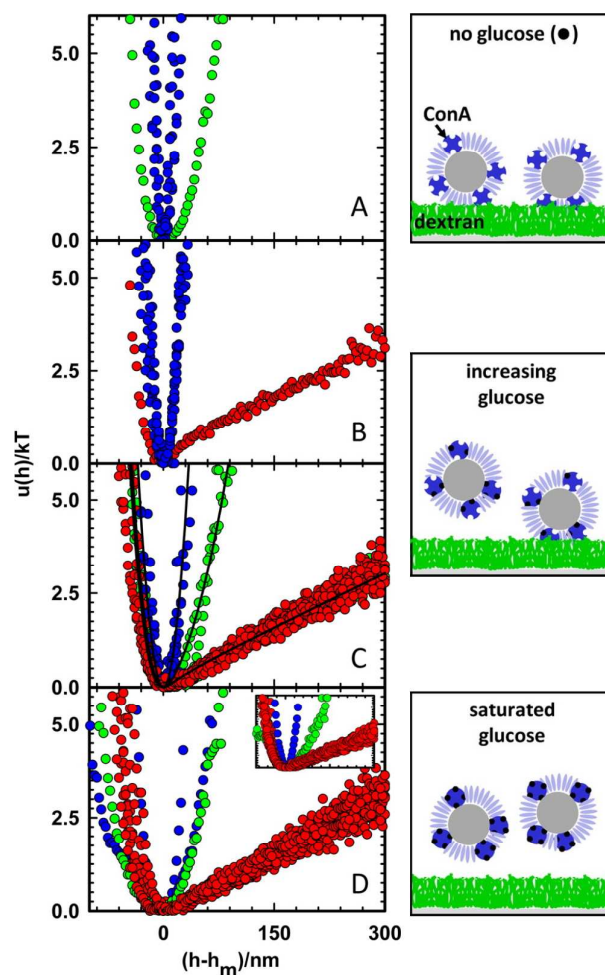


Fig. 13. Potential energy profiles between ConA-decorated colloids and dextran-modified surfaces. The bulk glucose concentrations [g] were (a) 0, (b) 5, (c) 10, and (d) 100 mM. Inset in panel (d) is interactions between BSA decorated colloids (no ConA) and dextran-functionalized surfaces as a control experiment. Measured potentials are color coded as (red) freely diffusing particles with short binding lifetimes, (green) loosely tethered particles with intermediate binding lifetimes, (blue) tightly bound particles with long binding lifetimes. Fig.13c shows theoretical curve fits including gravity, van der waals attraction, steric repulsion and tether potential. (Adopted and reproduced with the permission from ref. 77. Copyright (2013) American Chemical Society.)

5. Conclusions and perspective

In summary, by using single-particle force microscopy, TIRM, the interactions between designed colloidal surfaces with the presence or absence of macromolecules/nanoparticles can be successfully measured. Moreover, as the probe is purely excited by thermal energy, TIRM is sensitive and invasive optical technique for resolving sub $k_B T$ interaction with resolution down to nanometer, which is important in nano- and micro-technologies. This review demonstrates the use of TIRM in measuring depletion interaction, steric repulsion and bridging/tether attractions between the particle-surface mediated by polymers, polyelectrolytes, micelles and nanoparticles with different softness. We also discuss its applications in studying the non-specific and specific interactions between proteins and protein-carbohydrate in some biological systems. In future, a number of potential applications and improvements in using TIRM can be made, including the following issues:

Firstly, unequivocal TIRM measurements rely on surface chemistry of the colloidal particles. In this way, how to perform modification of particle surface in a controllable way is an important issue for widely use of TIRM measurements. Thanks to the progressive standardization of protocols in creating biocompatible surfaces by grafting/coating with proteins and other biomolecules, TIRM can be a more powerful technique in exploration of the interactions in biological systems.

Secondly, correction and exploration of the relationship between the scattered intensity of the evanescent wave I and the distance h from the bottom interface, especially in metallic surface, promise much wider applications of TIRM. In typical TIRM measurements, an exponential decay relationship between I and h was assumed. However, this relationship is valid under constrained conditions such as small penetration depth, large h , p polarization of incident light, *etc*⁸⁰⁻⁸². A novel experimental method was invented by Volpe *et al.* to determine the relationship between I and h ⁸³. This method relies only on the hydrodynamic interactions between the colloid and surface, and can allow precise measurements even in the highly reflected metallic surfaces.

Thirdly, theoretical description of polymer/nanoparticles induced interactions needs further improvements to be complemented with practical TIRM results. Examples include the description of depletion interaction between colloids induced by soft and charged nanoparticles^{13, 38, 60}, as well as the theoretical basis predicting the complex interactions induced by polyelectrolytes⁵⁸. On the basis of these well described interactions, those interactions under interest such as the specific interactions in biological systems can be accurately profiled.

Fourthly, a derived technique of TIRM, the Total Internal Reflection Fluorescence (TIRF) which utilizes evanescent wave to excite fluorescence of dyed probes, is expected to extend the related applications on accurate interaction and spatial measurements. Actually, TIRF has been widely used in observing biological objects and dynamics near wall because it remarkably improved signal/noise ratio compared with normal fluorescence methods.⁸⁴⁻⁸⁶ In contrast with TIRM, the use of fluorescence probes might lead to a complex convolution with the evanescent wave, which affects the spatial determination of the probes in TIRF⁸⁷. Additionally, the evanescent wave created through high-NA objective in TIRF has the problem to determine the penetration depth accuracy^{88, 89}. Nevertheless, theoretical exploration of the relationship between the scattered fluorescent intensity and the spatial distance from the surface in TIRF is expected to consummate due to its increasing applications.

Finally, a novel approach to study the rheological properties of complex fluid and soft matter using a combination of TIRM and magnetic tweezers has been presented by our group³¹. We essentially employ the evanescent wave generated in the total internal reflection microscopy (TIRM)) to trace and probe the displacement of an embedded paramagnetic probe particle (of a few micrometers diameter) near a solid surface. By measuring the instant scattered intensity, this technique allows tracking of the motion of the embedded particle perpendicular to the solid surface to a precision of nanometers, making it a highly sensitive spatial detector. Moreover, the integration of a magnetic driving force into the TIRM enables us to effectively manipulate the embedded particle in three dimensions by an oscillatory force so that

the local viscoelastic properties of the suspensions can be measured by resolving the particle motion. This microrheology technique thus provides a different way to precisely detect the local mechanics and structures of soft matter or complex suspensions near a solid surface.

Acknowledgement

The financial support of this work by the Hong Kong Special Administration Region (HKSAR) General Research Fund (CUHK402712, 2130304), and the NSFC/RGC Joint Research Scheme sponsored by the Research Grants Council of Hong Kong and the National Natural Science Foundation of China (N-CUHK454/11, 2900350) is gratefully acknowledge.

Notes and references

1. W. B. Russel, D. A. Saville and W. R. Schowalter, *Colloidal dispersions*, Cambridge University Press,, Cambridge ; New York, 1989.
2. L. D. L. B. Derjaguin, *Acta Phys. Chim. USSR*, 1941, **14**, 633.
3. J. T. G. O. E. J. W. Verwey, *Theory of the Stability of Lyophobic Colloids*, Elsevier, Amsterdam, 1948.
4. S. Block and C. A. Helm, *Physical Review E*, 2007, **76**.
5. N. C. Christov, K. D. Danov, Y. Zeng, P. A. Kralchevsky and R. von Klitzing, *Langmuir*, 2010, **26**, 915-923.
6. J. N. Israelachvili, *Intermolecular and surface forces*, Academic Press, Burlington, MA, 2011.
7. R. S. Farinato and P. Dubin, *Colloid-polymer interactions : from fundamentals to practice*, Wiley,, New York, 1999.
8. Y. Snir and R. D. Kamien, *Science*, 2005, **307**, 1067-1067.
9. A. Milling and S. Biggs, *Journal of Colloid and Interface Science*, 1995, **170**, 604-606.
10. Y. N. Ohshima, H. Sakagami, K. Okumoto, A. Tokoyoda, T. Igarashi, K. B. Shintaku, S. Toride, H. Sekino, K. Kabuto and I. Nishio, *Physical Review Letters*, 1997, **78**, 3963-3966.
11. E. Freyssingeas, K. Thuresson, T. Nylander, F. Joabsson and B. Lindman, *Langmuir*, 1998, **14**, 5877-5889.
12. P. Richetti and P. Kékicheff, *Physical Review Letters*, 1992, **68**, 1951-1954.
13. A. Sharma and J. Y. Walz, *J Chem Soc Faraday T*, 1996, **92**, 4997-5004.
14. X. J. Gong, X. C. Xing, X. L. Wei and T. Ngai, *Chinese J Polym Sci*, 2011, **29**, 1-11.
15. D. Kleshchanok, R. Tuinier and P. R. Lang, *Langmuir*, 2006, **22**, 9121-9128.
16. L. Helden, R. Roth, G. H. Koenderink, P. Leiderer and C. Bechinger, *Physical Review Letters*, 2003, **90**, 048301.
17. P. G. deGennes, *Macromolecules*, 1980, **13**, 1069-1075.
18. R. R. Netz and D. Andelman, *Phys Rep*, 2003, **380**, 1-95.
19. A. K. Dolan and S. F. Edwards, *Proceedings of the Royal Society A: Mathematical, Physical and Engineering Sciences*, 1974, **337**, 509-516.
20. J. Klein, *Nature*, 1980, **288**, 248-250.
21. S. J. Oshea, M. E. Welland and T. Rayment, *Langmuir*, 1993, **9**, 1826-1835.
22. M. A. Bevan and D. C. Prieve, *Langmuir*, 2000, **16**, 9274-9281.
23. D. Kleshchanok and P. R. Lang, *Langmuir*, 2007, **23**, 4332-4339.
24. W. A. Ducker, T. J. Senden and R. M. Pashley, *Nature*, 1991, **353**, 239-241.
25. H. J. Butt, *Biophysical Journal*, 1991, **60**, 1438-1444.
26. D. C. Prieve and B. M. Alexander, *Science*, 1986, **231**, 1269-1270.
27. D. C. Prieve, F. Luo and F. Lanni, *Faraday Discuss*, 1987, **83**, 297-307.
28. D. C. Prieve, *Advances in Colloid and Interface Science*, 1999, **82**, 33.
29. T. D. Iracki, D. J. Beltran-Villegas, S. L. Eichmann and M. A. Bevan, *Langmuir*, 2010, **26**, 18710-18717.
30. T. D. Edwards and M. A. Bevan, *Langmuir*, 2012, **28**, 13816-13823.

31. X. Gong, L. Hua, C. Wu and T. Ngai, *The Review of scientific instruments*, 2013, **84**, 033702.
32. H. Chew, D. S. Wang and M. Kerker, *Appl Optics*, 1979, **18**, 2679-2687.
33. S. Asakura and F. Oosawa, *The Journal of chemical physics*, 1954, **22**, 1255-1256.
34. D. Kleshchanok, R. Tuinier and P. R. Lang, *Journal of Physics: Condensed Matter*, 2008, **20**, 073101.
35. W. Knoblen, N. Besseling and M. Cohen Stuart, *Physical Review Letters*, 2006, **97**, 068301.
36. E. S. Pagac, R. D. Tilton and D. C. Prieve, *Langmuir*, 1998, **14**, 5106-5112.
37. P. C. Odiachi and D. C. Prieve, *Colloid Surface A*, 1999, **146**, 315-328.
38. J. Y. Walz and A. Sharma, *Journal of Colloid and Interface Science*, 1994, **168**, 485-496.
39. M. Piech and J. Y. Walz, *J Colloid Interface Sci*, 2000, **225**, 134-146.
40. S. Alexander, *Journal De Physique*, 1977, **38**, 983-987.
41. B. V. Derjaguin, *Kolloid Zeits*, 1934, **69**, 155-164.
42. S. Block and C. A. Helm, *J Phys Chem B*, 2008, **112**, 9318-9327.
43. L. Maggi, L. Segale, M. L. Torre, E. O. Machiste and U. Conte, *Biomaterials*, 2002, **23**, 1113-1119.
44. I. Banerjee, R. C. Pangule and R. S. Kane, *Adv Mater*, 2011, **23**, 690-718.
45. C. Bechinger, D. Rudhardt, P. Leiderer, R. Roth and S. Dietrich, *Physical Review Letters*, 1999, **83**, 3960-3963.
46. X. Wei, X. Gong and T. Ngai, *Langmuir*, 2013, **29**, 11038-11045.
47. X. Xing, G. Sun, Z. Li and T. Ngai, *Langmuir*, 2012, **28**, 16022-16028.
48. X. Xing, Z. Li and T. Ngai, *Macromolecules*, 2009, **42**, 7271-7274.
49. F. Jin, J. Ye, L. Z. Hong, H. F. Lam and C. Wu, *J Phys Chem B*, 2007, **111**, 2255-2261.
50. F. Jin, J. F. Li, X. D. Ye and C. Wu, *J Phys Chem B*, 2007, **111**, 11745-11749.
51. F. Jin, X. Gong, J. Ye and T. Ngai, *Soft Matter*, 2008, **4**, 968-971.
52. M. Piech and J. Y. Walz, *J Colloid Interface Sci*, 2002, **253**, 117-129.
53. A. Dobrynin and M. Rubinstein, *Progress in Polymer Science*, 2005, **30**, 1049-1118.
54. H. Tanaka, L. Odberg, L. Wagberg and T. Lindstrom, *Journal of Colloid and Interface Science*, 1990, **134**, 219-228.
55. M. R. Bohmer, O. A. Evers and J. M. H. M. Scheutjens, *Macromolecules*, 1990, **23**, 2288-2301.
56. R. R. Navarro, S. Wada and K. Tatsumi, *Separ Sci Technol*, 2003, **38**, 2327-2345.
57. O. A. Evers, G. J. Fleer, J. M. H. M. Scheutjens and J. Lyklema, *Journal of Colloid and Interface Science*, 1986, **111**, 446-454.
58. X. Gong and T. Ngai, *Langmuir*, 2013, **29**, 5974-5981.
59. Y. Yue, F. Jin, R. Deng, J. Cai, Y. Chen, M. C. Lin, H. F. Kung and C. Wu, *Journal of controlled release : official journal of the Controlled Release Society*, 2011, **155**, 67-76.
60. A. Sharma, S. N. Tan and J. Y. Walz, *Journal of Colloid and Interface Science*, 1997, **191**, 236-246.
61. X. Wei and T. Ngai, *Polymer Chemistry*, 2012, **3**, 2121-2128.
62. O. Azzaroni, A. A. Brown and W. T. S. Huck, *Advanced Materials*, 2007, **19**, 151-154.

63. X. Wei, X. Gong and T. Ngai, *Polymer Chemistry*, 2013, **4**, 4356-4365.
64. G. M. Liu, D. Wu, C. C. Ma, G. Z. Zhang, H. F. Wang and S. H. Yang, *Chemphyschem : a European journal of chemical physics and physical chemistry*, 2007, **8**, 2254-2259.
65. Z. X. Gu, Y. Yuan, J. L. He, M. Z. Zhang and P. H. Ni, *Langmuir*, 2009, **25**, 5199-5208.
66. A. Kusumo, L. Bombalski, Q. Lin, K. Matyjaszewski, J. W. Schneider and R. D. Tilton, *Langmuir*, 2007, **23**, 4448-4454.
67. W. N. Everett, H. J. Wu, S. G. Anekal, H. J. Sue and M. A. Bevan, *Biophys J*, 2007, **92**, 1005-1013.
68. R. Kurrat, J. E. Prenosil and J. J. Ramsden, *Journal of Colloid and Interface Science*, 1997, **185**, 1-8.
69. M. A. Bevan and D. C. Prieve, *Langmuir*, 1999, **15**, 7925-7936.
70. H. Brenner, *Chem. Engr. Sci.*, 1961, **16**, 242-251.
71. A. J. C. Goldman, R. G.; Brenner, H., *Chem. Engr. Sci.*, 1967, **22**, 637-651.
72. A. Potanin and W. Russel, *Physical Review E*, 1995, **52**, 730-737.
73. W. N. Everett, D. J. Beltran-Villegas and M. A. Bevan, *Langmuir*, 2010, **26**, 18976-18984.
74. D. Haussinger, T. Ahrens, T. Aberle, J. Engel, J. Stetefeld and S. Grzesiek, *Embo J*, 2004, **23**, 1699-1708.
75. S. Sivasankar, W. Brieher, N. Lavrik, B. Gumbiner and D. Leckband, *P Natl Acad Sci USA*, 1999, **96**, 11820-11824.
76. W. Baumgartner, P. Hinterdorfer, W. Ness, A. Raab, D. Vestweber, H. Schindler and D. Drenckhahn, *P Natl Acad Sci USA*, 2000, **97**, 4005-4010.
77. S. L. Eichmann, G. Meric, J. C. Swavola and M. A. Bevan, *Langmuir*, 2013.
78. S. B. Smith, L. Finzi and C. Bustamante, *Science*, 1992, **258**, 1122-1126.
79. C. Bustamante, J. F. Marko, E. D. Siggia and S. Smith, *Science*, 1994, **265**, 1599-1600.
80. L. Helden, E. Eremina, N. Riefler, C. Hertlein, C. Bechinger, Y. Eremin and T. Wriedt, *Appl Optics*, 2006, **45**, 7299-7308.
81. C. Hertlein, N. Riefler, E. Eremina, T. Wriedt, Y. Eremin, L. Helden and C. Bechinger, *Langmuir*, 2008, **24**, 1-4.
82. C. T. McKee, S. C. Clark, J. Y. Walz and W. A. Ducker, *Langmuir*, 2005, **21**, 5783-5789.
83. G. Volpe, T. Brettschneider, L. Helden and C. Bechinger, *Optics express*, 2009, **17**, 23975-23985.
84. T. Funatsu, Y. Harada, M. Tokunaga, K. Saito and T. Yanagida, *Nature*, 1995, **374**, 555-559.
85. D. Zenisek, J. A. Steyer and W. Almers, *Nature*, 2000, **406**, 849-854.
86. A. Yildiz, J. N. Forkey, S. A. McKinney, T. Ha, Y. E. Goldman and P. R. Selvin, *Science*, 2003, **300**, 2061-2065.
87. H. Brutzer, F. W. Schwarz and R. Seidel, *Nano Lett*, 2012, **12**, 473-478.
88. A. L. Mattheyses and D. Axelrod, *Journal of biomedical optics*, 2006, **11**, 014006.
89. C. Gell, M. Berndt, J. Enderlein and S. Diez, *J Microsc-Oxford*, 2009, **234**, 38-46.